Agricultural Water Management 230 (2020) 105953

Contents lists available at ScienceDirect

Agricultural Water Management

journal homepage: www.elsevier.com/locate/agwat

Influence of mulched drip irrigation on landscape scale evapotranspiration from farmland in an arid area

Zhenyu Zhang[a,b,c], Xiaoyu Li[a,b,*], Lijuan Liu[a,b], Yugang Wang[b], Yan Li[a,b]

[a] State Key Laboratory of Subtropical Silviculture, Zhejiang A&F University, Hangzhou, 311300, Zhejiang, China
[b] State Key Laboratory of Desert and Oasis Ecology, Xinjiang Institute of Ecology and Geography, Chinese Academy of Sciences, Urumqi, 830011, Xinjiang, China
[c] School of Geographic and Oceanographic Sciences, Nanjing University, Nanjing, 210023, Jiangsu, China

ARTICLE INFO

Keywords:
Mulched drip irrigation
Mulched border irrigation
Evapotranspiration
SEBAL model
Temperature-vegetation dryness index

ABSTRACT

Water-saving irrigation measures in arid areas affect evapotranspiration (ET) processes while conserving water. Mulched drip irrigation is considered the most efficient irrigation method because it distributes water uniformly in the soil, restricts deep percolation, and minimizes unproductive evaporation from soil. The effect of mulched drip irrigation on farmland ET during the growing season at a landscape scale remains unclear, despite being vital for developing optimal water resource management strategies in arid areas. To compare the effects of mulched drip irrigation and mulched border irrigation on ET, based on Landsat satellite imagery (2007–2009 with mulched border irrigation, and 2014–2016 with mulched drip irrigation), an improved Surface Energy Balance Algorithm for Land (SEBAL) model was used to evaluate ET for the two periods of an oasis at Sangong River Basin in the arid region of Northwest China. The results show that daily ET rates from farmland managed under mulched drip irrigation were on average 0.2–1 mm.d^{-1} higher than under mulched border irrigation between June and August. Correspondingly, the net radiation flux (R) increased 73.32 W·m^{-2} on average, and R was found to be the main determinant of the ET differences. Meanwhile, the average land surface albedo decreased by 20%, and negatively correlated with R ($P < 0.05$), indicating that the land surface albedo was the main factor affecting R. Furthermore, the Normalized Difference Vegetation Index (NDVI) exhibited a significant correlation with land surface albedo. More importantly, the Temperature–Vegetation Dryness Index (TVDI) under mulched drip irrigation was found to be approximately 21% lower than that under mulched border irrigation, indicating that the soil moisture conditions of the farmland under mulched drip irrigation was significantly improved compared to mulched border irrigation. Namely, less water stress resulted in better developed canopy of the crops, which in turn captured more radiation and thus increased ET. In the end, the observed increases in landscape-scale ET under mulched drip irrigation in arid area resulted from enhanced productivity of the crops due to lessened drought stress.

1. Introduction

Evapotranspiration (ET) is an important process in terrestrial water and energy cycle. As such, quantifying ET improves understanding of the water cycle and hydrological processes in terrestrial ecosystems (Stocker and Raible, 2005). The implementation of highly efficient agricultural water-saving measures undoubtedly has a significant effect on the water cycle in agricultural regions. Compared to other hydrological processes in the land-surface water cycle, the relationship between ET and agricultural water-saving measures is arguably more sensitive and direct (Mccabe and Wood, 2006).

Methods for estimating ET are mainly divided into two categories–those using direct instrumentation and those using remote sensing. The instrument-based methods include the lysimeter method (Lopez-Urrea et al., 2012), Bowen ratio method (Holland et al., 2013), eddy-correlation method (Ding et al., 2013) and scintillation flux meter method (Hoedjes et al., 2002; Watts et al., 2000). The first three of these methods are widely used for ET measurement at the field scale (Rana and Katerji, 2000). In comparison, the scintillation flux meter is more suitable for ET measurement at larger scales (> 10 km^2). Remote sensing measure ET indirectly via various models, such as the Surface Energy Balance Algorithm for Land (SEBAL) model (Bastiaanssen et al., 1998a, b; Zamani Losgedaragh and Rahimzadegan, 2018), Surface Energy Balance System (SEBS) model (Ma et al., 2012; Timmermans et al., 2013), Mapping Evapotranspiration with Internalized Calibration (METRIC) model (Allen et al., 2011) and three-temperature model (Qiu,

* Corresponding author at: State Key Laboratory of Subtropical Silviculture, Zhejiang A&F University, Hangzhou, 311300, Zhejiang, China.
E-mail address: lixy76@163.com (X. Li).

https://doi.org/10.1016/j.agwat.2019.105953
Received 11 July 2019; Received in revised form 30 November 2019; Accepted 1 December 2019

2015). Compared to instrument-based methods, remote sensing provides an effective means of estimating ET over larger spatial scales. Furthermore, remote sensing can help determine spatial and temporal patterns in ET. The SEBAL model, which is based on remote sensing data, has been widely used for ET estimation around the world. For example, Rahimzadegan and Janani (2019) used the SEBAL model to estimate ET rates for pistachio crops in Iran, achieving a higher coefficient of determination ($R^2 = 0.8$) than direct measurements. Bhattarai and Liu (2019) tested the validity of the SEBAL model using flux sites in Nebraska, USA, and found that the model could predict ET with a high degree of accuracy (the coefficient of determination between estimated ET and measured values ranged between 0.78 and 0.89). Ochege et al. (2019) successfully estimated ET in the Aral Sea Basin using Landsat 7 Enhanced Thematic Mapper (ETM) data in the SEBAL model, founding that estimated and directly measured ET values were well correlated (R^2 ranged from 0.94 to 0.98). Thus, previous research demonstrates that the SEBAL model performs well across a range of settings.

Mulched drip irrigation combines the drip irrigation and mulching techniques, which has been developed since the mid-1990s to become the predominant irrigation method in arid regions in China (Li et al., 2019; Xing et al., 2019). Drip irrigation is considered the most efficient irrigation method because it maintains a more uniform and stable distribution of water throughout the cropping cycle in accordance with crop water consumption, and limits deep percolation in comparison with furrow and flood irrigation (Karlberg et al., 2007).

Plastic mulching is an important element that helps improve the quality and efficiency of drip irrigation (Massatbayev et al., 2016). Compared to drip irrigation, mulched drip irrigation greatly reduces evaporation from unproductive soil evaporation and significantly alters ecohydrological processes in agroecosystems (Z. Wang et al., 2019; C. Wang et al., 2019; Zhao et al., 2017). Most existing studies have focused on crop yield and water use efficiency (WUE) under mulched drip irrigation conditions, the results of which show that this technique can increase crop yield and WUE to varying degrees (Bai et al., 2015; Li et al., 2018; H. Liu et al., 2017; M. Liu et al., 2017; Yang et al., 2017; Zhang et al., 2017a, b, 2017c). Comparisons between ET from mulched and non-mulched croplands under furrow or flooding irrigation have also been documented (Zegada-Lizarazu and Berliner, 2011; Shukla and Shrestha, 2015; Yang et al., 2018; Chen et al., 2019; Feng et al., 2019). In general, plastic film mulching has been shown to reduce ET and alter ET components as soil evaporation is decreased and crop transpiration is increased. However, the effect of plastic film mulching on ET under drip irrigation has rarely been studied as this technology is not widely applied in many countries, being most common in water-scarce countries such as Israel and China.

In the very few studies that have focused on the effect of mulched drip irrigation on ET, most have measured ET without comparison with other irrigation methods. For example, ET was estimated to be 538 mm during the entire cotton growing season under mulched drip irrigation from early-April through mid-October in 2009 at an oasis in northern Xinjiang, Northwest China, and the average daily ET rate reached 4.3–4.7 mm in July (Zhou et al., 2012). At the same oasis, the mean cumulative ET during the cotton-growing season under mulched drip irrigation was estimated to be 501 mm between 2009 and 2013, and the peak daily ET rate ranged between 5.9 and 6.5 mm (Bai et al., 2015). Experiments of mulched drip irrigation with brackish water in a cotton field in southern Xinjiang showed that the ET amount during the flowering and bolling irrigation stages accounted for 98.6% of the total ET (Li et al., 2016). A comparison of field-scale maize ET between mulched border irrigation and mulched drip irrigation indicated that total ET (over the entire cropping season) was 10% lower under mulched drip irrigation, while daily average ET rates were almost equal (Qin et al., 2016). However, the transferability of these field-scale observations to the landscape scale remains untested.

This study aimed to apply a modified SEBAL model to estimate ET under different irrigation methods during different years and explore the possible mechanisms for any observed differences. Our specific objectives were to: (1) compare ET from the same farmland region for periods under mulched drip-irrigation and mulched border irrigation management; and (2) investigate the factors controlling ET differences under these two irrigation methods.

2. Materials and methods

2.1. Study region

China's water resource is extremely scarce, with a per capita resource only a quarter of the world average. At the same time, agriculture accounts for 80% of China's water resource uses. Furthermore, the spatial distribution of water resources in China is unbalanced; more than 80% of China's water resources are located in the south of the country. Xinjiang, as the largest province, is located in the northwest region of China and is the largest arid area in the country. With the continuous development of the local economy, the conflict between water supply and demand has become increasingly prominent in Xinjiang. Agriculture accounts for 95% of the total water use in Xinjiang. To relieve the problem of this water shortage, a series of water-saving irrigation measures have been applied in agricultural production, with mulched drip-irrigation being the most popular one (Ibragimov et al., 2007; Wang et al., 2014).

Our study was carried out in the Sangong River Basin (SRB), Xinjiang, NW China (latitude: 44°00′–44°30′N; longitude: 87°40′–88°20′E). The Sangong River originates from the northern slopes of the TianShan Mountains. The elevation along the basin decreases from 750 m (in the southern region) to 450 m (in the northern region) above sea level. Passing through plain oases in its middle reaches, the river reaches the southern edge of the Gurbantunggut Desert and has a total length of around 80 km. The basin is a mountain-oasis-desert landscape, typical of the region (Li et al., 2013). Oases, being more productive than the surrounding deserts, are irrigated by water from the TianShan Mountains (Fig.1). The climate is an arid continental climate. Based on 30 years (1980–2010) of climatology data from a meteorological dataset, the mean annual temperature in this basin is 7.3 °C and the annual precipitation is approximately 160 mm, with an annual evaporation rate from a modified class A pan of approximately 1000 mm. In this basin, the agricultural mainly depends on irrigation due to limited precipitation and high evapotranspiration, and the precipitation contributes vary little to the agricultural water use (Wang et al., 2018). Hence, we can assume that the climatic conditions are similar between the two studying periods (2007–2009 and 2014–2016).

Farmland was digitally extracted to study the effects of different irrigation methods on ET. To ensure consistency between years, unchanged farmland was selected as the study area. As the main crop types in the study area are corn, wheat, and sunflowers, and the phonological period of wheat is different from those main crops, wheat fields were excluded from the analysis to eliminate the influence caused by the difference in crop types. The distribution of farmland in the study area is shown in Fig. 1. The irrigation system in this region changed from mulched border irrigation to mulched drip irrigation in 2010. Two Bowen ratio observation stations were established in the region (at 44°19′48″ N, 87°53′24″ E, in a sunflower field, and 44°21″36″ N, 87°52′12″ E, in a corn field) to measure daily ET amounts during 2016 under mulched drip irrigation. The observed parameters include net radiant flux, soil heat flux, temperature, humidity, wind speed, wind direction and precipitation.

The cultivation stage of cropland is a significant factor affecting ET. Based on the local statistical yearbooks, the planting proportions of the major crop types (corn, wheat, sunflowers and seed melon) were calculated during the two irrigation periods. During the mulched border irrigation period, the planting proportions of corn, wheat, sunflowers and seed melon were 11.3%, 21.6%, 36.4%, and 30.7%, respectively, compared to 11.5%, 22.1%, 34.1%, and 32.3%, respectively, during the

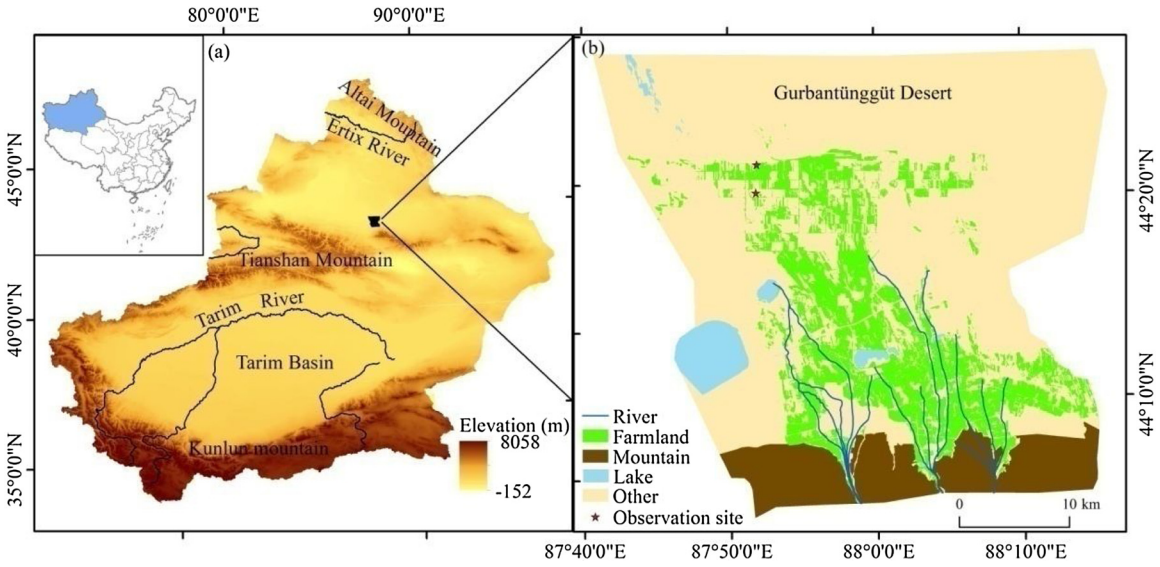

Fig. 1. Location of the study region in Xinjiang, China (a), and the main land cover types in the Sangong River Basin (b); farmland is highlighted in green (For interpretation of the references to colour in this figure legend, the reader is referred to the web version of this article).

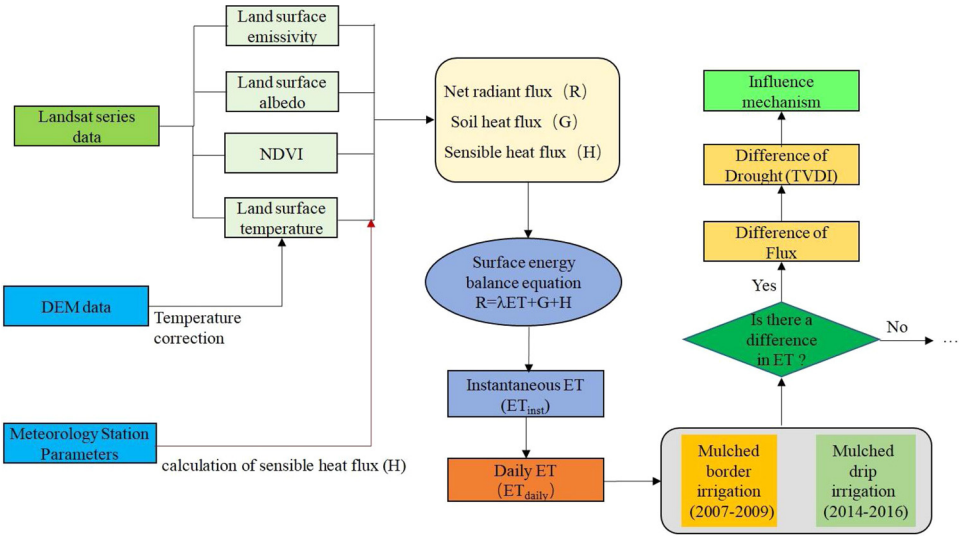

Fig. 2. The flowchart for comparing the farmland ET between the mulched border irrigation period and mulched drip irrigation period.

mulched drip irrigation period. This demonstrated that the proportions of the main crop types were very similar between the two study periods. The crop planning density was also comparable between the two irrigation periods in this region. The influence of crop type on ET was, therefore, negligible between the two irrigation periods and as such, was not considered further. The flowchart for comparing the farmland ET between the mulched border irrigation period and mulched drip irrigation period was presented in Fig. 2.

2.2. Datasets

Landsat 5 Thematic Mapper and Landsat 8 Operational Land Imager and Thermal Infrared Sensor (OLI/TIRS) datasets were acquired from the U.S. Geological Survey (https://glovis.usgs.gov/). The spatial resolution of the image data was 30 m and the time resolution was 16 days. Landsat 5 T M data were obtained for 2007, 2008, and 2009 (when mulched border irrigation was the dominant irrigation method), and Landsat 8 OLI/TIRS data were obtained for 2014, 2015, and 2016 (when mulched drip irrigation was the dominant method). As the cloud cover percentage of the imagery needs to be sufficiently low (< 15%) and consistent between years, a total of nine images were used for each irrigation period. Since the resolution of the Landsat 8 satellite data was 30 m, which is well above the width of mulch strips (approximately 0.8 m), soil surface temperature could not be distinguished between under mulch and outside mulch. Such heterogeneity in soil surface characteristics is often disregarded in large-scale studies (Cohen and Justice, 1999; Gallego-Sala et al., 2018; Kramer and Chadwick, 2018). Summary information for the imagery used in the study is provided in Table 1.

We also used ASTER GDEM V2 data to generate a digital elevation model (DEM) with a spatial resolution of 30 m. The DEM data were downloaded from the Geospatial Data Cloud (http://www.gscloud.cn/) of the Computer Network Information Center, Chinese Academy of Sciences.

2.3. Methodology

2.3.1. SEBAL model

The core element of the SEBAL model is the following surface energy balance equation:

Table 1
Specification of Landsat 5 and Landsat 8 data used in this study.

Date	Day of year (DOY)	Cloud cover (%)
2009/6/23	174	0.04
2009/7/9	190	1.95
2007/7/20	201	0
2009/7/25	206	0.34
2008/8/7	220	0.42
2008/8/23	236	10.85
2009/8/26	238	0.01
2016/6/26	178	1.1
2014/7/7	188	3.49
2016/7/12	194	8.73
2014/7/23	204	3.42
2015/7/26	207	6.2
2016/7/28	210	0.4
2014/8/8	220	13.32
2014/8/24	236	0.58
2016/8/29	242	0.62

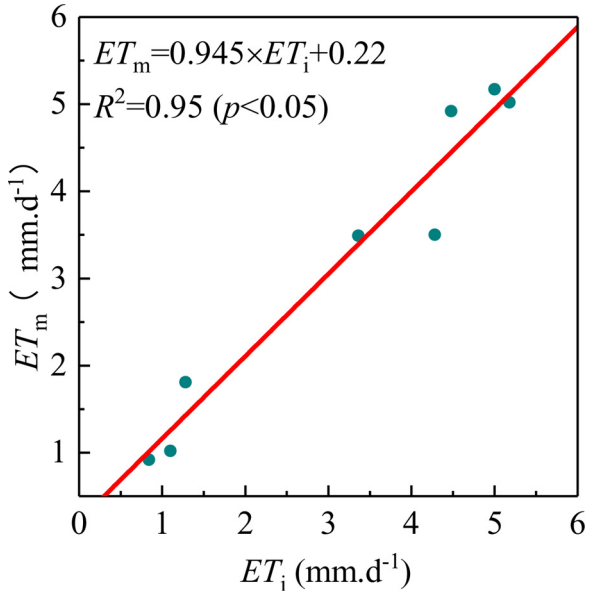

Fig. 3. Linear fitting between measured daily ET (ET_m) and inversed daily ET (ET_i).

$$R = G + H + \lambda ET \quad (1)$$

where $R$is the net radiation flux (W·m^{-2}); G is the soil heat flux (W·m^{-2}); $H$is the sensible heat flux (W·m^{-2}); λET is the latent heat flux (W·m^{-2}); λ is the latent heat of vaporization of water (usually 2.49 × 10^6 W·m^{-2} mm^{-1}); and $ET$is the evapotranspiration. *Requation reference goes here*reflects the amount of incoming solar energy absorbed by the surface and could be calculated using the following equation (Liebe et al., 1993):

$$R = (1 - a)R_{sd} + R_{ld} - R_{lu} - (1 - k)R_{ld} \quad (2)$$

where$a$ is the land surface albedo; R_{sd} is the shortwave solar radiation (W·m^{-2}); R_{ld} is the solar long-wave radiation (W·m^{-2}); R_{lu} is the land surface reflected long-wave radiation (W·m^{-2}); and k is the land surface emissivity.

Soil heat flux (G) is the amount of soil heat exchange per unit time and per unit area, which accounts for a small portion of the entire heat balance and can be calculated using the following equation (Bastiaanssen, 2000):

$$G = \frac{T_s - 273.16}{a} \times \left[0.0032 \times \frac{a}{c} + 0.0074\left(\frac{a}{c}\right)^2\right] \times (1 - 0.978NDVI^4) \times R \quad (3)$$

Where T_s is the land surface temperature (K); a is the land surface albedo; c is the impact of the satellite transit time on the soil heat flux; $NDVI$ is the normalized difference vegetation index.

Sensible heat flux (H) characterizes the heat exchange between the underlying surface and the atmosphere in a turbulent form, and is calculated as following (Bastiaanssen, 2000):

$$H = \frac{p_{air} C_p dT}{r_{ah}} \quad (4)$$

Where $P_{air}$is the air density (kg·m^{-3}); $C_p$is the specific heat of the air pressure (approximately 1004 J·kg^{-1}·K^{-1}); $dT$is the temperature difference between height Z_1 and Z_2 (Z_1 = 0.1 m, Z_2 = 2 m); and r_{ah} is the aerodynamic impedance. The selection of a hot spot and cold spot is a significant link in the calculation process of H. The process of spot selection was improved by Long and Singh (2013) and Bhattarai et al. (2017); the following steps constitute the improved selection processes used in this study:

(1) A hot spot is a pixel with a high surface temperature (in the top 1% of the T_s histogram) and no vegetation cover (NDVI < 0.1), and its latent heat flux is essentially zero.

(2) A cold spot is a pixel with a low surface temperature (in the lowest 1% of the T_s histogram) and high vegetation cover (NDVI > 0.6) If NDVI fails to meet the selection requirements, the homogeneous water body pixel in the area is selected as the cold spot.

(3) The hot spots and cold spots are selected in the area nearer the observation station and where the terrain is relatively flat (i.e., where the slope of the pixel surface was less than 15°).

The estimated daily ET (ET_i) was determined by instantaneous ET (ET_{inst}) as follows:

$$ET_{inst} = 3600 \times \frac{\lambda ET}{\lambda} \quad (5)$$

$$ET_i = \frac{2 \times N \times ET_{inst}}{\pi \times \sin\left(\frac{\pi \times t}{N-2}\right)} \quad (6)$$

where $\lambda ET$is the latent heat flux (W·m^{-2}); λ is the latent heat of vaporization of water; and N is sunshine duration (hours).

2.3.2. Calculation of the mean daily ET

The irrigation method of the study region was dominated by the mulched border irrigation before 2010, and from 2014 on, the mulched drip irrigation is the only irrigation method. The mean daily ET could be obtained by averaging the daily ET values of all pixels of farmland. It was calculated according to the following equation (Gautam and Raman, 2019):

$$ET_{mean} = \frac{SUM\,(ET_{pixel})}{K} \quad (7)$$

where ET_{mean} is the mean daily ET (mm·d^{-1}), ET_{pixel} is the daily ET value of each pixel of farmland (mm·d^{-1}); k is the total number of pixels of farmland; SUM (ET_{pixel}) is the sum of the daily ET of all pixels of farmland (mm·d^{-1}).

2.3.3. Temperature-vegetation dryness index (TVDI)

Soil drought is a dominant factor restricting regional ET. A low level of soil drought or high soil moisture content increases ET. Drought levels are quantified using various indices, such as the Palmer drought index (Sheffield et al., 2012), standardized precipitation ET index (Vicenteserrano et al., 2010) and TVDI (Sandholt et al., 2002). Among these, TVDI, is an effective indicator reflecting the soil moisture at large scale (Sandholt et al., 2002), has been widely applied at continental scale (Ali et al., 2019) and regional scale (Dinh Ngo et al., 2019; Holidi Armanto et al., 2019; Hu et al., 2018; Ling et al., 2019; Z. Wang et al., 2019; C. Wang et al., 2019). Thus, we used the TVDI to compare soil drought levels between 2009 and 2016. TVDI was calculated according to the following equation:

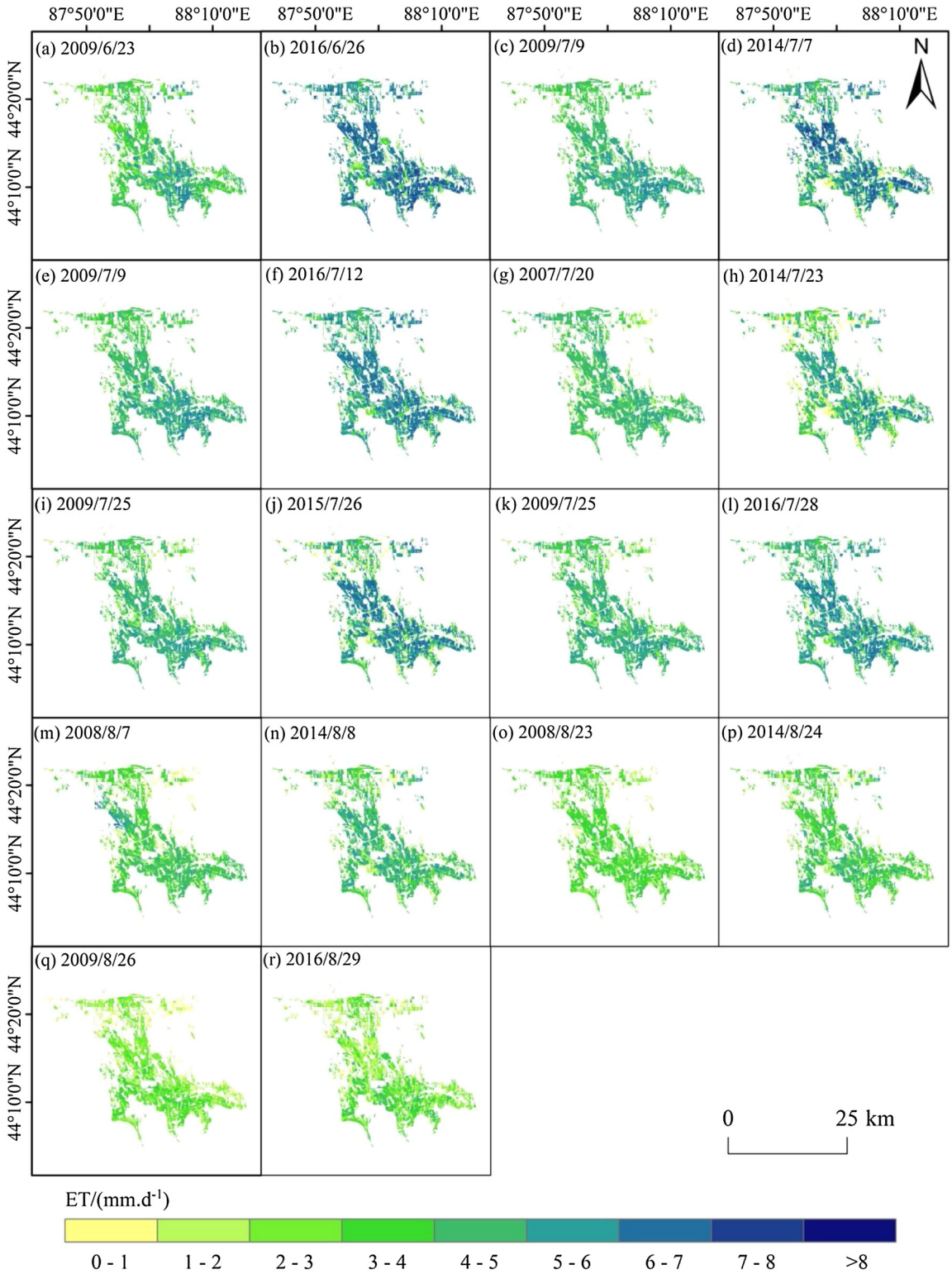

Fig. 4. Spatial distribution of daily ET for the same farmland under mulched border irrigation (2007–2009; a, c, e, g, i, k, m, o, and q) and mulched drip irrigation (2014–2016; b, d, f, h, j, l, n, p, and r). Plots for each irrigation method are shown in pairs for comparison.

$$T_{s\,\max} = \frac{T_s - T_{s\,\min}}{T_{s\,\max} - T_{s\,\min}} \tag{8}$$

where T_s is the land surface temperature of the pixel; $T_{s\,\max}$ is the maximum surface temperature corresponding to the pixel for the same vegetation index and comprising the dry edge of the T_s-NDVI eigenspace; and $T_{s\,\min}$ is the minimum surface temperature corresponding to the pixel for the same vegetation index and comprising the wet edge of the T_s-NDVI eigenspace. The dry and wet edge equation can be expressed as follows:

$$T_{s\,\max} = a_1 + b_1 \times \mathrm{NDVI} \tag{9}$$

$$T_{s\,\min} = a_2 + b_2 \times \mathrm{NDVI} \tag{10}$$

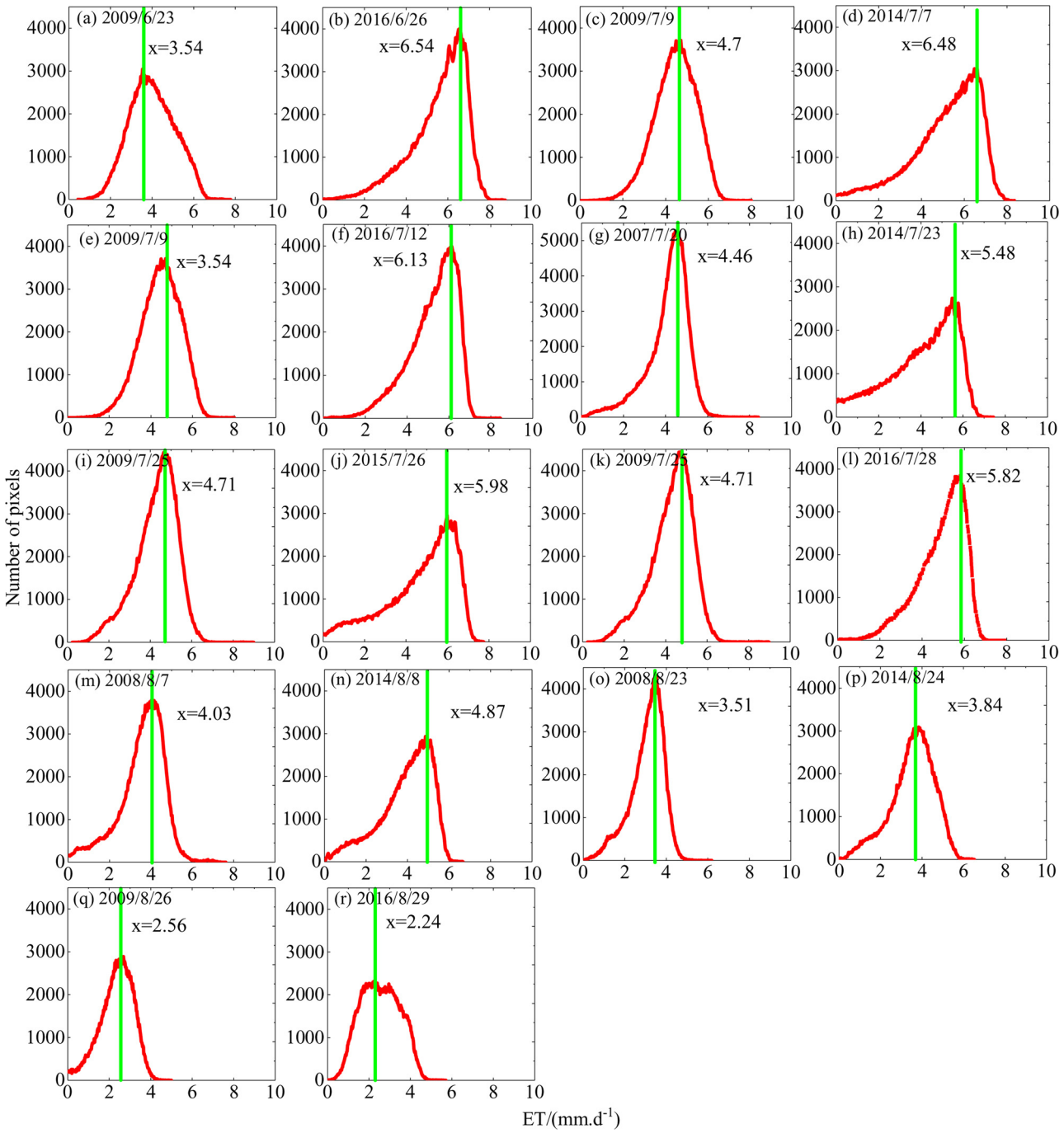

Fig. 5. Frequency distribution of daily ET for the periods 2007–2009 under mulched border irrigation (a, c, e, g, i, k, m, o, and q) and 2014–2016 under mulched drip irrigation (b, d, f, h, j, l, n, p, and r). Plots for each irrigation method are shown in pairs for comparison.

wherea_1, b_1, a_2, and $b_2$are the undetermined coefficients of the dry and wet edge equation, respectively. The values of the TVDI range from 0 to 1 and the higher the value, the higher the level of drought and the lower the soil moisture content. Furthermore, a_1, b_1, a_2 and b_2 can be used in drought analysis based the following conditions:

(1) The smaller b_1 is, the greater the drought interval in the study area. The nearer $|b_1\text{-}b_2|$ is to 0, the more severe the drought is in the study area.

(2) The nearer the absolute value of b_1 is to 0, the less drought there is and the more water there is in the soil.

(3) The higher the value of $|b_1\text{-}b_2|$, the greater the difference in the degree of drought and the more uneven the distribution of water is in the study area.

3. Results

3.1. Spatial distribution and temporal variation of daily ET

To validate the SEBAL model, a total of eight measured daily ET values (ET_m) from 2016 were compared with values from corresponding days estimated by the model (ET_i) (Fig.3). The coefficient of determination (R^2) between ET_m and ET_i was higher than 0.9, indicating that the SEBAL model produced reliable estimates of ET in the study region.

The spatial and frequency distributions of daily ET during the mulched border irrigation period (2007–2009) and the mulched drip irrigation period (2014–2016) are shown in Fig.4 and Fig.5, respectively. Daily ET values range from 2 to 6 mm·d^{-1} with higher rates

Table 2
Daily mean ET (ET_{mean}) and average NDVI under mulched border irrigation (2007–2009) and mulched drip irrigation (2014–2016).

Mulched border irrigation period			Mulched drip irrigation period		
Date	ET_{mean} ($mm{\cdot}d^{-1}$)	Average NDVI	Date	ET_{mean} ($mm{\cdot}d^{-1}$)	Average NDVI
2009/6/23	4.01	0.349	2016/6/26	5.07	0.443
2009/7/9	4.46	0.385	2014/7/7	5.14	0.398
2009/7/9	4.46	0.385	2016/7/12	5.24	0.449
2007/7/20	4.11	0.386	2014/7/23	4.51	0.455
2009/7/25	4.30	0.349	2015/7/26	4.71	0.394
2009/7/25	4.30	0.349	2016/7/28	4.92	0.384
2008/8/7	3.56	0.318	2014/8/8	3.93	0.425
2008/8/23	3.08	0.326	2014/8/24	3.55	0.354
2009/8/26	2.35	0.296	2016/8/29	2.56	0.298

occurring in the central part of the study region. Simultaneously, the ET frequency distribution revealed significant differences in daily ET on the corresponding days between the mulched drip irrigation period and the mulched border irrigation period. The average peak daily ET values during the two periods are given in Fig. 4, which shows that the values for mulched drip irrigation period are almost always higher than the mulched border irrigation period. Mean daily ET of each period also followed this trend (Table 2). The greatest differences in daily ET between the two irrigation periods occurred in June (a difference of approximately 1.06 $mm.d^{-1}$), followed by July (0.668 $mm.d^{-1}$), and August (0.36 $mm{\cdot}d^{-1}$), all differences were statistically significant ($p < 0.05$). The multi-year results reveal that ET during the mulched drip irrigation period was higher than that during the mulched border irrigation period during the crop growing season (June to August).

3.2. R, G, H, and λET under mulched border irrigation and mulched drip irrigation

Fig.6 shows distinct temporal changes in *R*, *G*, *H*, and λ*ET*. *R* increased between June and July and then decreased to a low level, while *G* showed a decreasing trend over time. *H* showed an upward trend over time and λ*ET* changed in a similar way to *R*, indicating that *R* was the main factor affecting ET (Bruemmer et al., 2012). To verify this, we calculated the correlation coefficient between each pair of the four surface fluxes (*R*, *G*, *H*, and λ*ET*) during the different irrigation period (Fig.7). The correlation coefficient, which is calculated by using the average value of each flux in corresponding days, between the average values of *R* and λ*ET* was 0.96 during the mulched border irrigation period and 0.95 during the mulched drip irrigation period. As such, *R* was the main factor affecting ET irrespective of the method of irrigation used.

Furthermore, Fig.6 indicates that in general, *R*, *G*, *H*, and λ*ET* under mulched drip irrigation were higher than under mulched border irrigation. This indicates that mulched drip irrigation increased these fluxes to varying degrees during the main crop growing season; *R* was 15% higher (73.32 $W{\cdot}m^{-2}$), *G* was 17% higher (17.88 $W{\cdot}m^{-2}$), and *H* was 18% higher (12.44 $W{\cdot}m^{-2}$). Since *R* was the dominant factor affecting ET and it showed the greatest difference between the irrigation periods, the average λ*ET* and daily ET of farmland with mulched drip irrigation were generally higher than with mulched border irrigation.

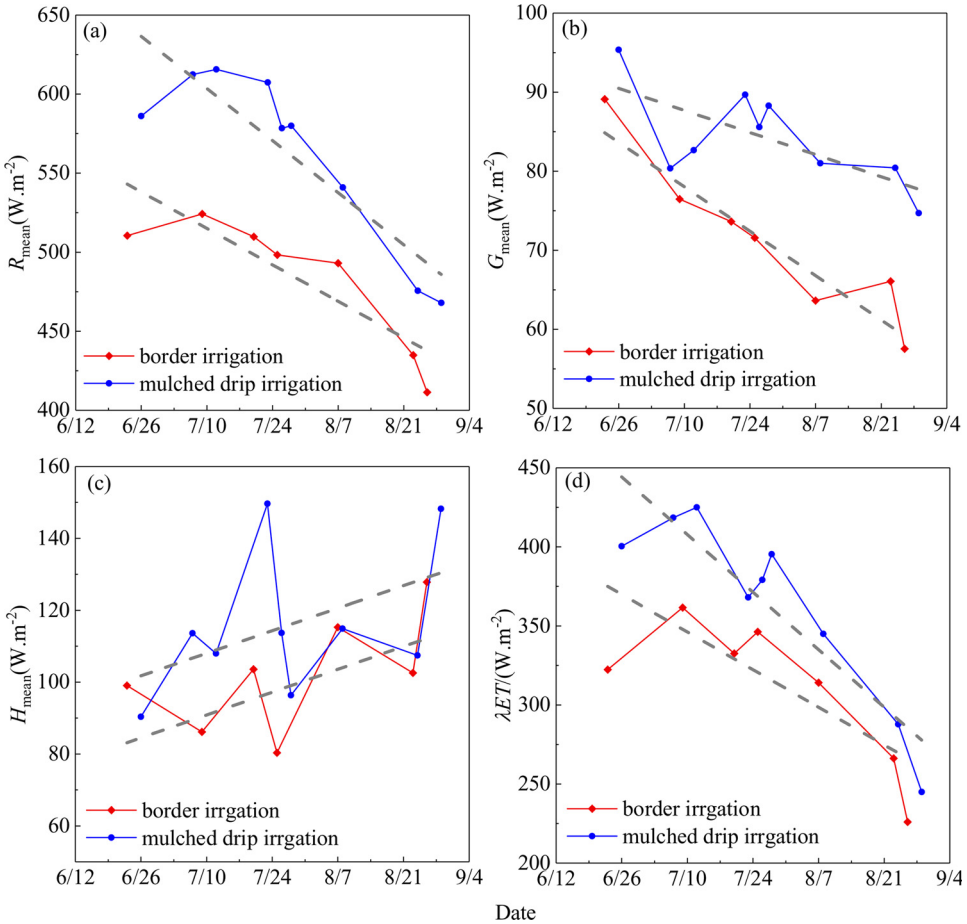

Fig. 6. Variation in surface energy flux during the mulched border and mulched drip irrigation periods: (a) net radiation flux (R_{mean}); (b) mean soil heat flux (G_{mean}); (c) sensible heat flux (H_{mean}); and (d) latent heat flux (λET_{mean}).

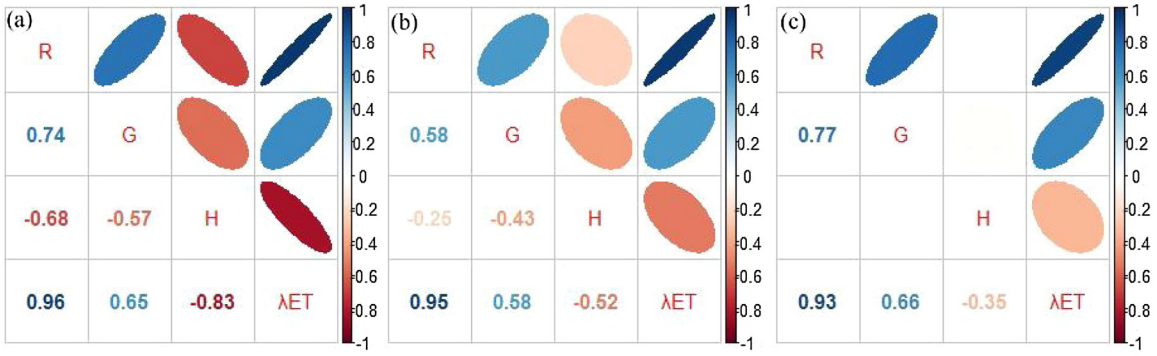

Fig. 7. Correlation coefficient between each pair of the four surface energy fluxes (*R*, *G*, *H*, and λ*ET*) during (a) the mulched border irrigation period (2007–2009), (b) the mulched drip irrigation period (2014–2016), and (c) both irrigation periods (2007–2009 and 2014–2016).

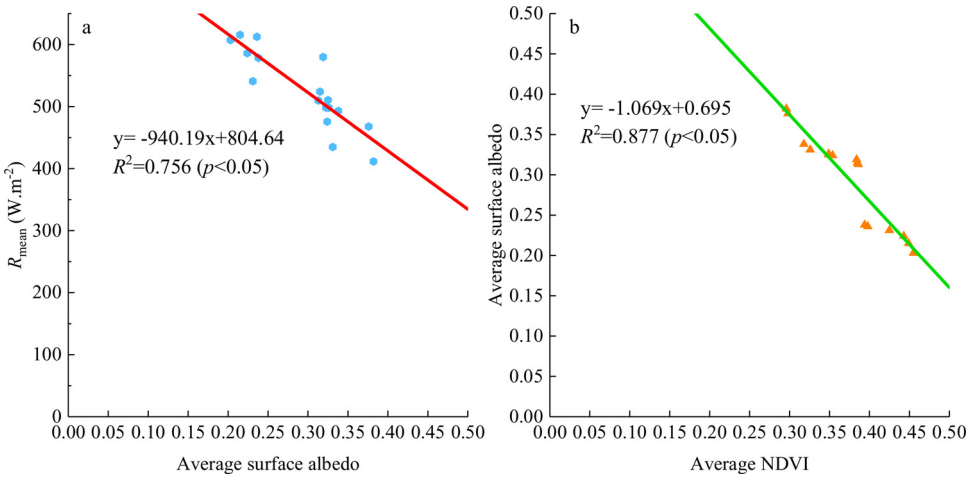

Fig. 8. Relationships between R_{mean} and average surface albedo (a) and average surface albedo and average NDVI (b).

Table 3
Spatially averaged average TVDI during the mulched border irrigation period (2007–2009) and the mulched drip irrigation period (2014–2016).

mulched border irrigation period		mulched drip irrigation period	
Date	Average TVDI	Date	Average TVDI
2009/6/23	0.48	2016/6/26	0.40
2009/7/9	0.52	2014/7/7	0.38
2009/7/9	0.52	20167/12	0.40
2007/7/20	0.41	2014/7/23	0.38
2009/7/25	0.42	2015/7/26	0.41
2009/7/25	0.42	2016/7/28	0.39
2008/8/7	0.70	2014/8/8	0.40
2008/8/23	0.54	2014/8/24	0.42
2009/8/26	0.62	2016/8/29	0.48

3.3. Factors contributing to difference in R between irrigation methods

The amount of *R* was identified as the main factor controlling the difference in ET between the two irrigation methods. The higher the *R* is, the more solar energy is available for photosynthesis and transpiration. Land surface albedo, which indicates the amount of solar energy reflects back to the atmosphere from the land surface (Blonquist et al., 2010; Samarasinghe, 2003; Singh et al., 2016), is also closely related to *R*; higher land surface albedo results in lower *R*. This is demonstrated by a significant negative correlation between R_{mean} and the average land surface albedo ($p < 0.05$, Fig.8a). The average land surface albedo during the mulched border irrigation period was 0.329, which is 20% higher than during the mulched drip irrigation period (0.263). Farmland managed under mulched drip irrigation can, therefore, absorb relatively more solar energy, which results in higher *R* values.

In addition, land surface albedo is affected by surface characteristics. As our study focused on the crop growing season, the farmland surface was mainly covered by the crop canopy. Thus, we speculated that surface albedo should be correlated with NDVI, which is an indicator of vegetation cover. Indeed, surface albedo was significantly negatively correlated with NDVI ($p < 0.05$, Fig.8b). This indicates that NDVI values obtained during the mulched drip irrigation period were higher than during the mulched border irrigation period.

Generally, crop growth is enhanced under mulched drip irrigation comparing to mulched border irrigation, which reduces land surface albedo and increases *R*, and subsequently results in higher daily ET.

3.4. Soil drought levels under different irrigation methods

Table 3 shows that the average TVDI values for the farmland under mulched drip irrigation were appropriately 0.05 to 0.2 lower than that under mulched border irrigation. This indicates that mulched drip irrigation reduced drought stress in crops in comparison to mulched border irrigation.

Simultaneously, the T_s-NDVI eigenspaces plotted in Fig.9 further indicate a lower level of drought under mulched drip irrigation. First, the dry edge undetermined coefficient

(b_1) during the mulched drip irrigation period was greater than that during the mulched border irrigation period ($b_1$during the mulched border irrigation period: -22, -26.19, -13.08, -21.78, -14.09, -18.91, and -19.57; $b_1$during the mulched drip irrigation period: -14.19, -22.09, -15.69, -22.54, -17.64, -18.19, -21.55, -18.29, and -14.06). Second, the values of $|b_1 - b_2|$ during the mulched drip irrigation period were lower than during the mulched border irrigation period ($|b_1-b_2|$ during the

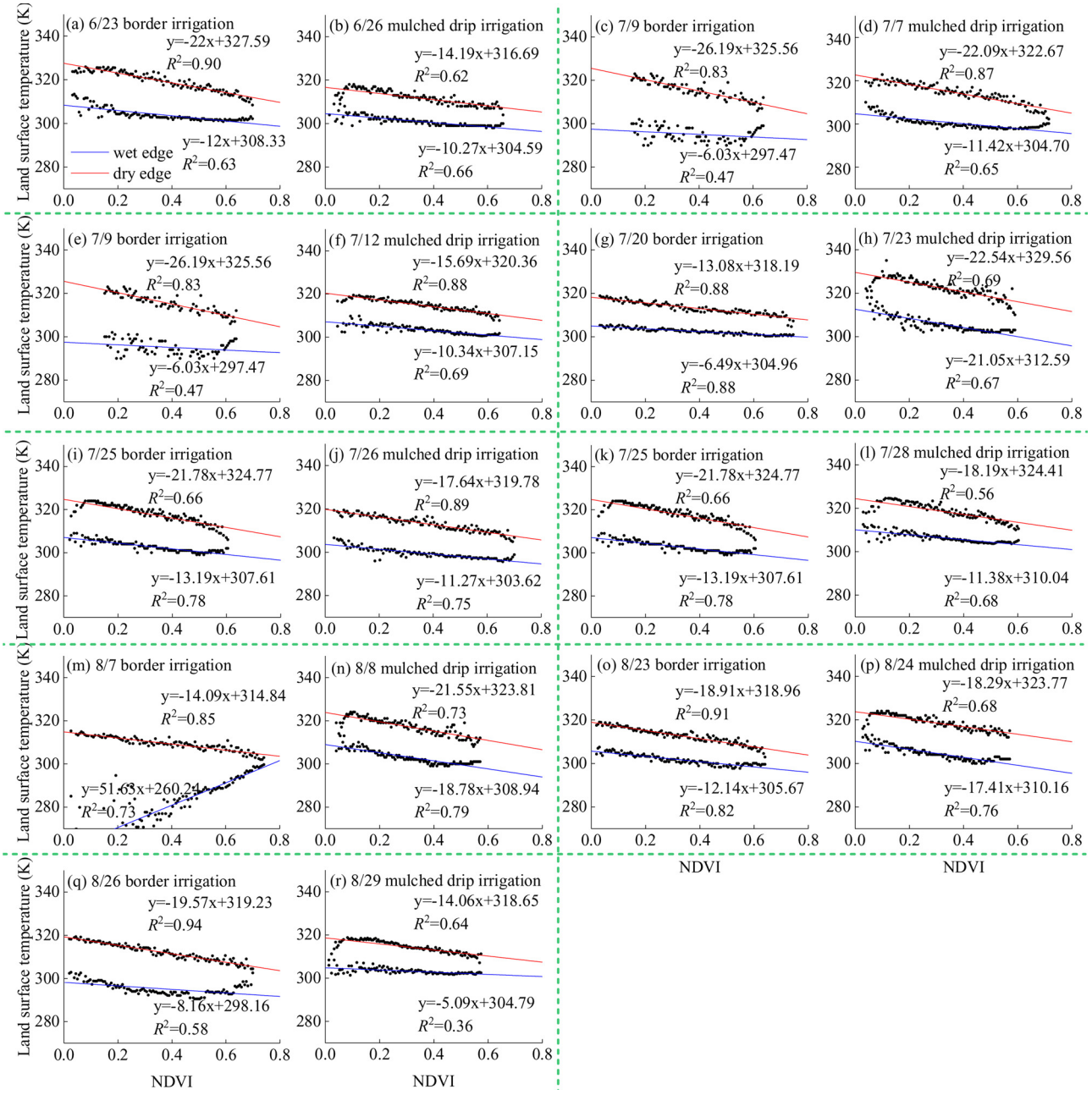

Fig. 9. T_s-NDVI eigenspace for the same farmland under mulched border irrigation (a, c, e, g, i, k, m, o, and q) and mulched drip irrigation (b, d, f, h, j, l, n, p, and r).

Table 4
Potential evapotranspiration (ET_p) and precipitation (Pre) between June and August during the mulched border irrigation and mulched drip irrigation periods.

	ET_p (mm)						Pre (mm)					
	Mulched border irrigation period			Mulched drip irrigation period			Mulched border irrigation period			Mulched drip irrigation period		
	2007	2008	2009	2014	2015	2016	2007	2008	2009	2014	2015	2016
June	197.4	200.5	143.3	154.9	111.2	157.7	8.3	6.9	16.2	6.7	30.2	31.5
July	184.1	181	186.6	184.1	199.6	170.8	61.2	23	11.3	5.1	2.1	30
August	152.7	158	173.7	164.7	155.3	166.7	42.2	17	3.7	1.2	32	12.2
Annual total	999.2	979.7	923	939	847.1	884.5	225.5	117.9	185.6	123.7	197.6	248.5
Annual Average	967.3			890.2			176.3			189.93		

Table 5
Irrigation details during the mulched border irrigation and mulched drip irrigation periods.

Irrigation mode	Irrigation interval	Irrigation volume	Irrigation times
Mulched border irrigation	15 days	510 mm	5
Mulched drip irrigation	10 days	376 mm	8

mulched border irrigation period: 10, 20.16, 6.59, 8.59, 37.54, 6.77, and 11.41; $|b_1\text{-}b_2|$ during the mulched drip irrigation period: 3.92, 10.67, 5.35, 1.49, 6.37, 6.81, 2.77, 0.88, and 8.97). This illustrates that the distribution of soil water in the farmland under mulched drip irrigation was more uniform than under mulched border irrigation. Drip irrigation supplies water at high frequencies directly to the root zone in a restricted volume of soil, so that the soil moisture conditions for crops were generally better than under border irrigation.

4. Discussion

4.1. The relationship between precipitation and potential evapotranspiration

To compare the climatic conditions affecting ET during the different irrigation periods, local meteorology station data were used to summarize the evaporative demand (evaporation from a modified Class A pan) and precipitation between June and August (Table 4). The average total potential evapotranspiration (ET_p) during the period of mulched border irrigation was 525.8 mm (for the growing season), which was slightly higher than the period under mulched drip irrigation (488.3 mm, for the growing season). Although the ET_p of the farmland was slightly lower for the period under drip irrigation management, ET was higher during this period than the period under mulched border irrigation. This indicates that the difference in ET between the two periods was not caused by ET_p but by crop growth (as indicated by NDVI) (Yue et al., 2018; Zheng et al., 2019; Zou et al., 2018). On the other hand, Table 4 shows that the average total precipitation between June and August during the mulched border irrigation period was 63.27 mm, comparing to 50.33 mm during the mulched drip irrigation period. Despite this, the mean daily ET during the mulched drip irrigation period were higher, implying that precipitation was not the primary driver of ET in this irrigated farmland.

4.2. The effects of irrigation methods on ET

The details of the irrigation applied between June and August during the two periods are shown in Table 5. Mulched border irrigation consumed much more water than mulched drip irrigation (> 134 mm). However, previous studies indicated that the water loss rate (via leaching and soil evaporation) for mulched border irrigation in this region can exceed 50% compared to 10% under mulched drip irrigation (H. Liu et al., 2017; M. Liu et al., 2017). Therefore, a larger proportion of irrigation water couldn't be used by crops on mulched border irrigated farmland compared to farmland irrigated using mulched drip irrigation (Grebenyukov, 2002; Moavenshahidi et al., 2016). This results in less available water for ET in border irrigated farmland. Furthermore, between June and August, the crop canopy is fully closed and the evaporation from the soil surface is very limited (Naveen et al., 2019). Mulched drip irrigation can only limit the loss of water via evaporation from the soil, while transpiration can be enhanced due to improved crop growth (Liu et al., 2015). Thus, ET rates during the main crop growing season were typically higher under mulched drip irrigation than mulched border irrigation.

4.3. Sustainability of mulched drip irrigation

It is clear that mulched drip irrigation is an effective strategy for conserving water when compared to the more commonly applied border irrigation. On the one hand, mulched drip irrigation improves the crop growth, which results in a higher ET rate; while on the other hand, it improves the water use efficiency of farmland by limiting water loss. Some studies show that the proportion of water lost under mulched border irrigation can exceed 40% (Zheng et al., 2017) compared to 13% or lower under mulched drip irrigation (Umair et al., 2019). This means that a greater proportion of available water is taken up by crops under mulched drip irrigation, which enhanced crop growth. Thus, higher ET under mulched drip irrigation during the main crop growing season does not contradict the sustainability of this irrigation strategy with respect to water conservation.

5. Conclusion

To compare the farmland ET between mulched border irrigation period and mulched drip irrigation period, we used SEBAL model to evaluate ET for the two periods of the farmland in Sangong River Basin in northern Xinjiang, Northwest China. Daily ET values for farmland managed under mulched drip irrigation were higher than the same farmland managed under mulched border irrigation, with differences ranging from 0.36 to 1.06 $mm{\cdot}d^{-1}$. An increase in net radiation flux increased the daily ET rates during the mulched drip irrigation period. At the same time, NDVI showed a significant negative correlation with land surface albedo ($R^2 = 0.877$). The NDVI values of farmland under mulched drip irrigation were higher than that under mulched border irrigation, which resulted in a lower land surface albedo and increased R values. The TVDI and Ts-NDVI eigenspace results indicated that crops under mulched drip irrigation experienced, on average, lower levels of water stress compared to crops under mulched border irrigation. This improved water conditions and crop growth resulted in a denser and higher canopy (with correspondingly high NDVI values) that in turn captured more energy for transpiration. Thus, mulched drip irrigation can reduce unproductive water consumption by leaching and soil evaporation, and increases effective water use such as crop transpiration. As an advanced technology, drip-irrigation creates more favorable soil water conditions, enhances crop growth, and thereby increases ET rates.

Declaration of Conflict Interest

There are no conflicts of interest to declare.

Acknowledgments

This study was funded by the National Natural Science Foundation of China (No. U1503182, 31470708, 41501205 & 41271202).

References

Ali, S., Tong, D., Xu, Z.T., Henchiri, M., Wilson, K., Siqi, S., Zhang, J., 2019. Characterization of drought monitoring events through MODIS- and TRMM-based DSI and TVDI over South Asia during 2001-2017. Environ Sci Pollut Res. https://doi.org/10.1007/s11356-019-06500-4.

Allen, R., Irmak, A., Trezza, R., Hendrickx, J.M.H., Bastiaanssen, W., Kjaersgaard, J., 2011. Satellite-based ET estimation in agriculture using SEBAL and METRIC. Hydrol. Process. 25 (26), 4011–4027.

Bai, J., Wang, J., Chen, X., Luo, G., Shi, H., Li, L., Li, J., 2015. Seasonal and inter-annual variations in carbon fluxes and evapotranspiration over cotton field under drip irrigation with plastic mulch in an arid region of Northwest China. J. Arid Land 7 (2), 272–284.

Bastiaanssen, W.G.M., 2000. SEBAL-based sensible and latent heat fluxes in the irrigated

Gediz Basin. Turkey. J Hydrol 229 (1–2), 87–100.
Bastiaanssen, W.G.M., Menenti, M., Feddes, R.A., Holtslag, A.A.M., 1998a. A remote sensing surface energy balance algorithm for land (SEBAL). 1. Formulation. J. Hydrol. (Amst) 212 (1/4), 198–212.
Bastiaanssen, W.G.M., Pelgrum, H., Wang, J., Ma, Y., Moreno, J.F., Roerink, G.J., van der Wal, T., 1998b. A remote sensing surface energy balance algorithm for land (SEBAL).: part 2: validation. J. Hydrol. (Amst) 212 (1/4), 213–229.
Bhattarai, N., Quackenbush, L.J., Im, J., Shaw, S.B., 2017. A new optimized algorithm for automating endmember pixel selection in the SEBAL and METRIC models. Remote Sens. Environ. 196, 178–192.
Bhattarai, N., Liu, T., 2019. LandMOD ET mapper: a new matlab-based graphical user interface (GUI) for automated implementation of SEBAL and METRIC models in thermal imagery. Environ. Model. Softw. 118, 76–82.
Blonquist Jr., J.M., Allen, R.G., Bugbee, B., 2010. An evaluation of the net radiation submodel in the ASCE standardized reference evapotranspiration equation: implications for evapotranspiration prediction. Agr Water Manage 97, 1026–1038.
Bruemmer, C., Black, T.A., Jassal, R.S., Grant, N.J., Spittlehouse, D.L., Chen, B., Nesic, Z., Amiro, B.D., Arain, M.A., Barr, A.G., Bourque, C.P.A., Coursolle, C., Dunn, A.L., Flanagan, L.B., Humphreys, E.R., Lafleur, P.M., Margolis, H.A., McCaughey, J.H., Wofsy, S.C., 2012. How climate and vegetation type influence evapotranspiration and water use efficiency in Canadian forest, peatland and grassland ecosystems. Agr Forest Meteorol 153, 14–30.
Chen, Z., Sun, S., Zhu, Z., Jiang, H., Zhang, X., 2019. Assessing the effects of plant density and plastic film mulch on maize evaporation and transpiration using dual crop coefficient approach. Agric. Water Manage. 225, 105765.
Cohen, W.B., Justice, C.O., 1999. Validating MODIS terrestrial ecology products: linking in situ and satellite measurements. Remote Sens. Environ. 70 (1), 1–3.
Ding, R., Kang, S., Li, F., Zhang, Y., Tong, L., 2013. Evapotranspiration measurement and estimation using modified Priestley-Taylor model in an irrigated maize field with mulching. Agr Forest Meteorol 168, 140–148.
Dinh Ngo, T., Nguyen Thi Thu, H., Quy Tran, D., Koike, K., Nhuan Mai, T., 2019. Effective band ratio of landsat 8 images based on VNIR-SWIR reflectance spectra of topsoils for soil moisture mapping in a tropical region. Remote Sens. (Basel) 11.
Feng, Y., Hao, W., Gao, L., Li, H., Gong, D., Cui, N., 2019. Comparison of maize water consumption at different scales between mulched and non-mulched croplands. Agric. Water Manage. 216, 315–324.
Gallego-Sala, A.V., Charman, D.J., Brewer, S., Page, S.E., Prentice, I.C., Friedlingstein, P., Björck, S., 2018. Latitudinal limits to the predicted increase of the peatland carbon sink with warming. Nat. Clim. Chang. 8 (10), 907–913.
Gautam, A., Raman, B., 2019. Local gradient of gradient pattern: a robust image descriptor for the classification of brain strokes from computed tomography images. Pattern Anal. Appl. https://doi.org/10.1007/s10044-019-00838-8.
Grebenyukov, P.G., 2002. The choice of optimal model for calculating seepage losses from channels and rivers. Water Resour. 29 (5), 510–517.
Hoedjes, J.C.B., Zuurbier, R.M., Watts, C.J., 2002. Large aperture scintillometer used over a homogeneous irrigated area, partly affected by regional advection. Bound-lay Meteorol 105 (1), 99–117.
Holidi Armanto, M.E., Damiri, N., Putranto, D.D.A., 2019. Characteristics of selected peatland uses and soil moisture based on TVDI. J Eco Eng 20, 194–200.
Holland, S., Heitman, J.L., Howard, A., Sauer, T.J., Giese, W., Ben-Gal, A., Agam, N., Kool, D., Havlin, J., 2013. Micro-Bowen ratio system for measuring evapotranspiration in a vineyard interrow. Agr Forest Meteorol 177, 93–100.
Hu, X., Shi, L., Lin, L., Zhang, B., Zha, Y., 2018. Optical-based and thermal-based surface conductance and actual evapotranspiration estimation, an evaluation study in the North China Plain. Agr Forest Meteorol 263, 449–464.
Ibragimov, N., Evett, S.R., Esanbekov, Y., Kamilov, B.S., Mirzaev, L., Lamers, J.P.A., 2007. Water use efficiency of irrigated cotton in Uzbekistan under drip and furrow irrigation. Agr Water Manage 90 (1), 112–120.
Karlberg, L., Rockstrom, J., Annandale, J.G., Steyn, J.M., 2007. Low-cost drip irrigation – a suitable technology for southern Africa? Agric. Water Manage. 89, 59–70.
Kramer, M.G., Chadwick, O.A., 2018. Climate-driven thresholds in reactive mineral retention of soil carbon at the global scale. Nat. Clim. Chang. 8 (12), 1104–1108.
Li, M., Du, Y., Zhang, F., Bai, Y., Fan, J., Zhang, J., Chen, S., 2019. Simulation of cotton growth and soil water content under film-mulched drip irrigation using modified CSM-CROPGRO-cotton model. Agr Water Manage 218, 124–138.
Li, Q., Li, H., Zhang, S., 2018. Yield and water use efficiency of dryland potato in response to plastic film mulching on the Loess Plateau. Acta Agr Scand B-s P 68 (2), 175–188.
Li, X., Jin, M., Zhou, N., Huang, J., Jiang, S., Telesphore, H., 2016. Evaluation of evapotranspiration and deep percolation under mulched drip irrigation in an oasis of Tarim basin. China. Journal of Hydrology 538, 677–688.
Li, X., Wang, Y., Liu, L., Luo, G., Li, Y., Chen, X., 2013. Effect of land use history and pattern on soil carbon storage in arid region of Central Asia. PLoS One 8 (7), e68372.
Liebe, H.J., Hufford, G.A., Cotton, M.G., 1993. Propagation modeling of moist air and suspended water/ice particles at frequencies below 1000 GHz. Agard Specialists' Meeting of the Electromagnetic Wave Propagation Panel.
Ling, H., Guo, B., Zhang, G., Xu, H., Deng, X., 2019. Evaluation of the ecological protective effect of the "large basin" comprehensive management system in the Tarim River basin. China. Sci Total Environ 650, 1696–1706.
Liu, H., Wang, X., Zhang, X., Zhang, L., Li, Y., Huang, G., 2017. Evaluation on the responses of maize (Zea mays L.) growth, yield and water use efficiency to drip irrigation water under mulch condition in the Hetao irrigation District of China. Agr Water Manage 179, 144–157.
Liu, M., Yang, L., Li, F., Wang, S., 2017. Numerical simulation of field infiltration coefficient under different irrigation scheduling in Xinjiang. Chin Rural Water and Hydro 12 (1), 17–21.
Liu, Y., Li, Y., Li, J., Yan, H., 2015. Effects of mulched drip irrigation on water and heat conditions in field and maize yield in sub-humid region of northeast China. T Chin Soc Agric Mach 46 (10), 93–104.
Long, D., Singh, V.P., 2013. Assessing the impact of end-member selection on the accuracy of satellite-based spatial variability models for actual evapotranspiration estimation. Water Resour. Res. 49 (5), 2601–2618.
Lopez-Urrea, R., Montoro, A., Manas, F., Lopez-Fuster, P., Fereres, E., 2012. Evapotranspiration and crop coefficients from lysimeter measurements of mature' Tempranillo' wine grapes. Agr Water Manage 112, 13–20.
Ma, W., Hafeez, M., Rabbani, U., Ishikawa, H., Ma, Y., 2012. Retrieved actual ET using SEBS model from Landsat-5 TM data for irrigation area of Australia. Atmos. Environ. 59, 408–414.
Massatbayev, K., Izbassov, N., Nurabaev, D., Musabekov, K., Shomantayev, A., Massatbayev, M., 2016. Technology and regime of sugar beet drip irrigation with plastic mulching under the conditions of the jambyl region. Irrig. and Drain. 65, 620–630.
Mccabe, M.F., Wood, E.F., 2006. Scale influences on the remote estimation of evapotranspiration using multiple satellite sensors. Remote Sens. Environ. 105 (4), 271–285.
Moavenshahidi, A., Smith, R., Gillies, M., 2016. Seepage losses in the Coleambally Irrigation Area – loss estimates from channel automation data. Aust. J. Water Resour. 20 (1), 78–88.
Naveen, G., Eberbach, P.L., Humphreys, E., Balwinder, S., Sudhir, Y., Kukal, S.S., 2019. Estimating soil evaporation in dry seeded rice and wheat crops after wetting events. Agr Water Manage 217, 98–106.
Ochege, F.U., Luo, G., Obeta, M.C., Owusu, G., Duulatov, E., Cao, L., Nsengiyumva, J.B., 2019. Mapping evapotranspiration variability over a complex oasis-desert ecosystem based on automated calibration of Landsat 7 ETM+ data in SEBAL. GIsci. Remote Sens. 56, 1305–1332.
Qin, S., Li, S., Kang, S., Du, T., Tong, L., Ding, R., 2016. Can the drip irrigation under film mulch reduce crop evapotranspiration and save water under the sufficient irrigation condition? Agr Water Manage 177, 128–137.
Qiu, G.Y., 2015. Comparison of the three-temperature model and conventional models for estimating transpiration. Jpn. Agric. Res. Q. Jarq 36 (2), 73–82.
Rahimzadegan, M., Janani, A., 2019. Estimating evapotranspiration of pistachio crop based on SEBAL algorithm using Landsat 8 satellite imagery. Agr Water Manage 217, 383–390.
Rana, G., Katerji, N., 2000. Measurement and estimation of actual evapotranspiration in the field under Mediterranean climate: a review. Eur. J. Agron. 13 (2), 125–153.
Samarasinghe, G.B., 2003. Growth and yields of Sri Lanka's major crops interpreted from public domain satellites. Agr Water Manage 58, 145–157.
Sandholt, I., Rasmussen, K., Andersen, J., 2002. A simple interpretation of the surface temperature/vegetation index space for assessment of surface moisture status. Remote Sens. Environ. 79 (2), 213–224.
Sheffield, J., Wood, E.F., Roderick, M.L., 2012. Little change in global drought over the past 60 years. Nature 491 (7424), 435–438.
Shukla, S., Shrestha, N.K., 2015. Evapotranspiration for plastic-mulched production system for gradually cooling and warming seasons: measurements and modeling. Irrig. Sci. 33, 387–397.
Singh, A.K., Dubey, O.P., Ghosh, S.K., 2016. Irrigation scheduling using intervention of Geomatics tools-A case study of Khedli minor. Agr Water Manage 177, 454–460.
Stocker, Thomas F., Raible, Christoph C., 2005. Climate change: water cycle shifts gear. Nature 434 (7035), 830.
Timmermans, J., Su, Z., van der Tol, C., Verhoef, A., Verhoef, W., 2013. Quantifying the uncertainty in estimates of surface-atmosphere fluxes through joint evaluation of the SEBS and SCOPE models. Hydrol. Earth Syst. Sci. Discuss. 17 (4), 1561–1573.
Umair, M., Hussain, T., Jiang, H., Ahmad, A., Yao, J., Qi, Y., Zhang, Y., Min, L., Shen, Y., 2019. Water-saving potential of subsurface drip irrigation for winter wheat. Sustainability 11 (10), 1–15.
Vicenteserrano, S.M., Beguería, S., Lópezmoreno, J.I., 2010. A multiscalar drought index sensitive to global warming: the standardized precipitation evapotranspiration index. J Climate 23 (7), 1696–1718.
Wang, C., Chen, J., Chen, X., Chen, J., 2019. Identification of concealed faults in a grassland area in Inner Mongolia, china, using the temperature vegetation dryness index. J. Earth Sci. 30, 853–860.
Wang, Y., Deng, C., Liu, Y., Niu, Z., Li, Y., 2018. Identifying change in spatial accumulation of soil salinity in an inland river watershed. China. Sci Total Environ 621, 177–185.
Wang, Z.M., Jin, M.G., Simunek, J., van Genuchten, M.T., 2014. Evaluation of mulched drip irrigation for cotton in arid Northwest China. Irrigation Sci 32 (1), 15–27.
Wang, Z., Fan, B., Guo, L., 2019. Soil salinization after long-term mulched drip irrigation poses a potential risk to agricultural sustainability. Eur. J. Soil Sci. 70 (1), 20–24.
Watts, C.J., Chehbouni, A., Rodriguez, J.C., Kerr, Y.H., Hartogensis, O., Bruin, H.A.R.D., 2000. Comparison of sensible heat flux estimates using AVHRR with scintillometer measurements over semi-arid grassland in northwest Mexico. Agr Forest Meteorol 105 (1), 81–89.
Xing, X., Du, W., Ma, X., 2019. Field-scale distribution and heterogeneity of soil salinity in the mulched-drip-irrigation cotton field. Arch. Agron. Soil Sci. 65 (9), 1248–1261.
Yang, K., Wang, F., Shock, C.C., Kang, S., Huo, Z., Song, N., Ma, D., 2017. Potato performance as influenced by the proportion of wetted soil volume and nitrogen under drip irrigation with plastic mulch. Agr Water Manage 179, 260–270.
Yang, Y., Zhou, X., Yang, Y., Bi, S., Yang, X., Liu, D., 2018. Evaluating water-saving efficiency of plastic mulching in Northwest China using remote sensing and SEBAL. Agric. Water Manage. 209, 240–248.
Yue, P., Zhang, Q., Yang, Y., Zhang, L., Zhang, H., Hao, X., Sun, X., 2018. Seasonal and inter-annual variability of the Bowen smith ratio over a semi-arid grassland in the Chinese Loess Plateau. Agr Forest Meteorol 252, 99–108.

Zamani Losgedaragh, S., Rahimzadegan, M., 2018. Evaluation of SEBS, SEBAL, and METRIC models in estimation of the evaporation from the freshwater lakes (Case study: Amirkabir dam, Iran). J. Hydrol. (Amst) 561, 523–531.
Zegada-Lizarazu, W., Berliner, P.R., 2011. Inter-row mulch increase the water use efficiency of furrow-irrigated maize in an arid environment. J. Agronomy & Crop Science 237–248.
Zhang, G., Liu, C., Xiao, C., Xie, R., Ming, B., Hou, P., Liu, G., Xu, W., Shen, D., Wang, K., Li, S., 2017a. Optimizing water use efficiency and economic return of super high yield spring maize under drip irrigation and plastic mulching in arid areas of China. Field Crop Res 211, 137–146.
Zhang, Y.-L., Wang, F.-X., Shock, C.C., Yang, K.-J., Kang, S.-Z., Qin, J.-T., Li, S.-E., 2017b. Effects of plastic mulch on the radiative and thermal conditions and potato growth under drip irrigation in arid Northwest China. Soil Till Res 172, 1–11.
Zhang, Y.-L., Wang, F.-X., Shock, C.C., Yang, K.-J., Kang, S.-Z., Qin, J.-T., Li, S.-E., 2017c. Influence of different plastic film mulches and wetted soil percentages on potato grown under drip irrigation. Agr Water Manage 180, 160–171.
Zhao, W., Cui, Z., Zhang, J., Jin, J., 2017. Temporal stability and variability of soil-water content in a gravel mulched field in northwestern China. J. Hydrol. (Amst) 552, 249–257.
Zheng, C., Lu, Y., Guo, X., Li, H., Sai, J., Liu, X., 2017. Application of HYDRUS-1D model for research on irrigation infiltration characteristics in arid oasis of northwest China. Environ. Earth Sci. 76 (23), 785–795.
Zheng, H., Lin, H., Zhou, W., Bao, H., Zhu, X., Jin, Z., Song, Y., Wang, Y., Liu, W., Tang, Y., 2019. Revegetation has increased ecosystem water-use efficiency during 2000-2014 in the Chinese Loess Plateau: evidence from satellite data. Ecol. Indic. 102, 507–518.
Zhou, S., Wang, J., Liu, J., Yang, J., Xu, Y., Li, J., 2012. Evapotranspiration of a drip-irrigated, film-mulched cotton field in northern Xinjiang. China. Hydrol Process 26 (8), 1169–1178.
Zou, M., Zhong, L., Ma, Y., Hu, Y., Huang, Z., Xu, K., Feng, L., 2018. Comparison of two satellite-based evapotranspiration models of the Nagqu River Basin of the Tibetan Plateau. J Geophys Res-Atmos 123 (8), 3961–3975.